Surface and Volume Reconstruction of the Left Ventricle from SPECT data

Oscar García Panyella
CITEM
EA La Salle / Universitat Ramon Llull
C/ Quatre Camins 2, 08022 Barcelona
oscarg@salleURL.edu

Antoni Susín Sánchez
Departament de Matemàtica Aplicada I
Universitat Politècnica de Catalunya
Avda. Diagonal 647, 08028 Barcelona
Toni.Susin@upc.es

Abstract

This document describes the three-dimensional reconstruction of the internal and external surfaces of the human's left ventricle from actual SPECT data. The reconstruction is a first process fitting in a complete VR application that will serve as an important diagnosis tool for hospitals. Beginning with the surfaces reconstruction, the application will provide volume and interactive real-time manipulation to the model. We focus on speed, precision and smoothness for the final surfaces. As long as heart diseases diagnosis requires experience, time and professional knowledge, simulation is a key-process that enlarges efficiency.

Keywords

Tele-medicine, deformable models, virtual reality, image filters, 3D surface.

1. INTRODUCTION

Access to a 3D model obtained from patient's data can have several applications like support on diagnosis, surgery planning, student's training or even remote-operation. A first approximation to the problem would be using a manual process with specific image-processing software though it would require deep medical knowledge and experience.

Some parts of the human body like skin or bones have clear intensity-gradient variations that make surface-reconstruction techniques suitable. Unfortunately these techniques don't work when regions are formed from soft tissue. That's the case of the heart, liver or muscles.

In order to solve those cases several contour-based techniques have been introduced. In all the approximations the evolution is similar, an initial parametrically defined contour or mesh which deforms attracted to a certain energy minimum, numerically implemented as a finite difference method.

Another possible approach is to use the finite element method which gives nice results but is computationally expensive and complex.

The dynamic model that we present solves the same type of problems using the evolution of a deformable mesh affected by internal and external forces. Internal forces are defined in terms of elasticity; external forces are derived from the data set as a vector field called *Gradient Vector Flow* (*GVF*) [Xu97][Xu98].

The use of the *GVF* vector field avoids some of the limitations of traditional snakes related to initial distance to data and robustness in concave regions.

2. INPUT DATA

The system takes as its input SPECT, *Single Photon Emission Computed Tomography*, images. Those images give functionality keys about the organ and do not describe its anatomy. Thus data shows the activity being held in terms of the amount of useful tissue, without giving a clue about shape. From this knowledge it becomes clear that ischemic areas, it means in absence of blood irrigation, won't be shown in the images. That's the case of ventricle areas being affected by a heart attack.

3. INTERNAL FORCES

Internal forces define four possibilities for the model:

- *Plane deformation model*, where each of the triangles in the mesh has its own elasticity forces. Deformation will be characterized by the added action of three forces: stretch, shear and bend.

- *Spring-mass deformation model*, where the only internal force is stretch, defined between pairs of particles following *Hook*'s equation.

- *Restricted spring-mass deformation model*, where spring-forces are only allowed in the direction normal to the derived vector field.

- *Free deformation model*, where the only existing force is the external one, derived from the data set. There's no connectivity between particles and topology must be maintained using a smoothing algorithm, apart from the evolution scheme.

All the models have been extensively reported in [Amatller00], [García00] and [Susin01]. The smoothing algorithm can be found at [García02].

4. EXTERNAL FORCES

External forces consist on the minimization of a functional that mixes the information derived from the image-intensities gradient with a diffusion term that allows the vector field to be spread out.

The vector field that acts as the external force is then obtained by minimizing the functional shown in figure 1.

$$\varepsilon = \iiint \mu \sum_{i \in \{x,y,z\}} (u_i^2 + v_i^2 + w_i^2) + |\nabla I|^2 |V - \nabla I|^2 \, dxdydz$$

Figure 1: The energy-based functional [Xu97][Xu98].

The functional consists on two well-differentiated terms. On the left, the diffusion term that spreads the field when variations on intensities are negligible. On the right the property term, that dominates the expression when variations are important. The µ parameter will control the balance between both terms.

5. DYNAMIC EVOLUTION

The dynamic evolution is based on *Newtonian* classics, as it is shown in figure 2:

$$F_i = m_i \cdot \ddot{x}_i \begin{cases} \dot{x} = v \\ \dot{v} = F_i/m_i \end{cases}$$

Figure 2: Newtonian dynamics.

In order to solve the system, we need an appropriated numerical method. This method or solver, depends on the deformable model applied. We have used:

- Implicit *Euler*'s method when using the plane deformable model.

- Explicit methods like *Euler*, *Midpoint* or *Runge-Kutta-4* when using the spring-mass, restricted spring-mass and free deformation models.

Reports on these can be found at [Amatller00], [García00] and [Susin01].

6. TEST MODEL: the PHANTOM

In order to measure the reliability of the system from the results point of view, it becomes necessary to test a data set with known volume. The *PHANTOM* is a test-model that offers known geometry and volume, allowing us to compare with the obtained results. In our case we have used the one from the *Vall d'Hebron* Hospital which is presented in figure 3:
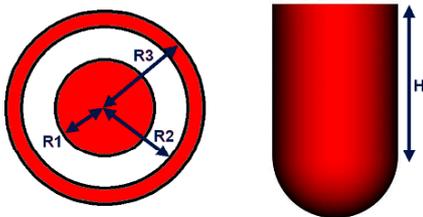

Figure 3: The PHANTOM dimensions.

With R1=20mm, R2==35mm, R3=45mm and H=55mm. Those distances give external and internal volumes of 305301.4 mm^3 and 89794 mm^3 respectively.

7. RESULTS

7.1 Oscillations

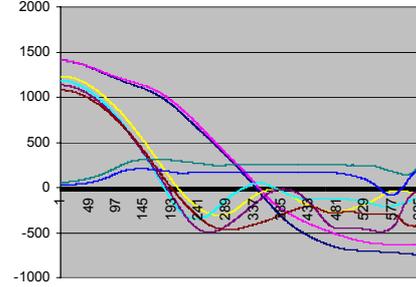If we analyse several particles trajectories:

Figure 4: Particles oscillate in data frontiers.

We can see the oscillation effect in the frontiers of the data. Figure 4 shows the distance between several particles and the data to be recovered. Defining the black line (0) as the zero-distance to data, it becomes clear that particles oscillate while system iterates, even if they have reached the surroundings of the data frontiers.

This behaviour demands for a stopping mechanism that we have implemented by using an accurate segmentation filter: the *Canny-Edge Detector* [Canny86], in order to mark the border voxels (data frontiers).
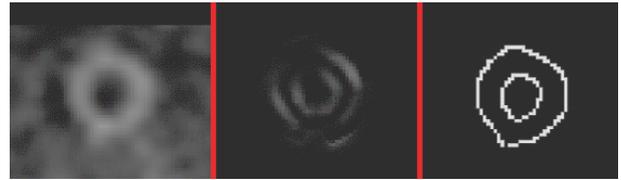

Figure 5: Original *SPECT* image (left), after *Reynolds* operator (middle) and after *Canny* operator (right).

Figure 5 shows some results. An appropriate tuning of the filter (1.8 for the Gaussian, 0.3 for the low threshold and 0.8 for the high threshold) ensures performance for *SPECT* images rather than using less sophisticated operators like the *Reynolds* gradient.

7.2 Distance to real data

We present a comparison between deformation models and final distance of the surface to data in table 1.

K and KD stand for constant and damping constant respectively.

Initial mesh consisted on 642 particles and 1280 triangles. We used a GVF balancing constant of 25.0 and a damping factor of 25%.

The implicit scheme (plane deformation) is clearly slower than the explicit one (spring-mass and free cases) but Δt can be bigger in the implicit methods. Despite we have used a smaller Δt for the explicit schemes they are faster even under those circumstances.

Note that the free model achieves 97% of the particles really close to data (less than one voxel) while the rest stays at the 75% approximately.

	Plane (1)	Plane (2)	Spring-Mass	Free
Δt	0.01 s.	0.05 s.	0.0005 s.	0.0005 s.
% < 1 voxel	77 %	74.5 %	73.6 %	97 %
K Stretch	10	10	10	---
KD Stretch	1	1	1	---
K Bend	10	10	---	---
KD Bend	1	1	---	---
K Shear	1	1	---	---
KD Shear	0.1	0.1	---	---

Table 1: Final distances depending on

the deformation model.

7.3 Size of triangles

The final 3D model, in the future, will consist both on surface and on internal volume. It will be necessary to perform a tetrahedralization between both surfaces, external and internal. This process, which will be a further step in our project, will permit the real-time interaction with the synthetic organ. Tetrahedralization will associate internal triangles with its external neighbours. Then it is imperative to ensure the final quality of the mesh, rejecting all possible degenerations.

A detailed mesh will recover data with minimal error but won't be smooth enough. On the contrary, if the initial triangle size is major or equal than the separation between data slices, we can ensure a good aspect ratio for the triangles (area / major edge).

	Flat shading	Gouraud shading	Averaged	Max	Min
1			84.03 / 5.1	170.02 / 7.73	23.15 / 1.99
2			22.5 / 2.57	116.4 / 5.24	0.82 / 0.09
3			6.24 / 1.29	72.38 / 4.95	0.0007 / 0.0005

Table 2: Reconstructions depending

on the LoD of the meshes (mm^2 / averaged).

Table 2 shows a recovered *PHANTOM* using three different meshes. First case (low LoD) does not present any degenerations. Second case (medium LoD) deals with some degenerations as we can derive from its minimal area value. Third case (high LoD) presents clear degeneration problems.

We conclude that the first mesh, where triangle dimensions are similar to space between data-slices, is smooth enough and gives not degenerations.

7.4 Volume estimation

Volume results are presented comparing the real data volume with the one reconstructed. We compute the real volume by filtering data voxels, rejecting those with intensities lower than 20% of the maximum.

If we quantify the data volume we obtain a value of 368782 mm^3. This volume differs from the theoretical one in a 12%. We must take in account the low resolution of the data and the error due to the quality of the reception from the medical equipment.
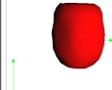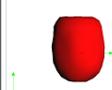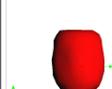
Flat shading	Gouraud shading	Error (%)	ΔT (s)	Time (s)	Solver
		1.44	0.1	0.322	Euler
		0.68	0.12	0.14	Mid Point
		1.53	0.17	0.111	RK4

Table 3: Volume results vs. numerical method.

Simulations on table 3 have been executed using the free deformation method with the smoothing algorithm active. The selected initial mesh is the one labelled as 2 in table 2. Third column shows the computed % of error between the recovered and the real data. All three numerical schemes are satisfactory achieving errors less than 2%.

7.5 A complete cardiac cycle reconstruction

Figure 6 presents a complete cardiac cycle recovered from actual patient's data. The cycle is formed by eight temporal acquisitions. Each data set consists on 64 x 64 x 24 voxels, with spatial resolutions of 2.87 mm (X), 2.87 mm (Y) and 5.74 mm (Z).

The meshes were generated using the free deformation model with the RK4 explicit scheme, using a GVF balancing constant of 10, a damping factor of 1% and a time increment Δt of 0.1 seconds.
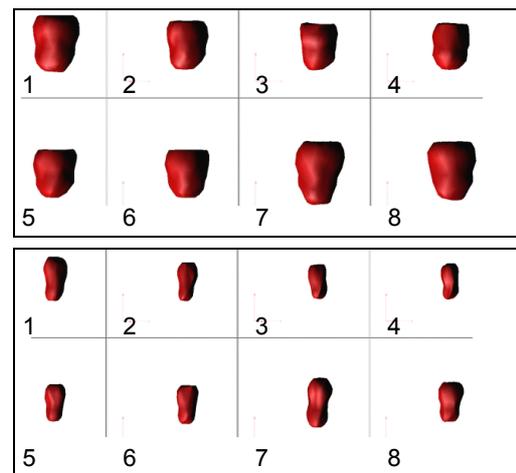
Figure 6: Complete cardiac cycle with external surfaces (top) and internal surfaces (bottom).

Table 4 presents internal, external and wall volumes in mm^3.

	1	**2**	**3**	**4**
Int.	74741	45677	36523	32956
Ext.	443762	316804	254112	250131
Wall	369021	271127	217589	217175
	5	**6**	**7**	**8**
Int.	47237	55825	79581	63133
Ext.	299779	345830	473608	451525
Wall	252542	290005	394027	388392

Table 4: Volumes for the eight temporal instances.

As a first diagnosis tool, physicians use the Ejection Fraction (EF) parameter. Figure 7 shows the parameter for the ventricle in figure 6:

$$EF(\%) = \frac{DiastoleEndVolume - SystoleEndVolume}{DiastoleEndVolume} x100 = 58.6\%$$

Figure 7: EF calculation equation.

Where all the volumes are internal. EF values inside the interval 50%-70% stay for a non-pathological situation.

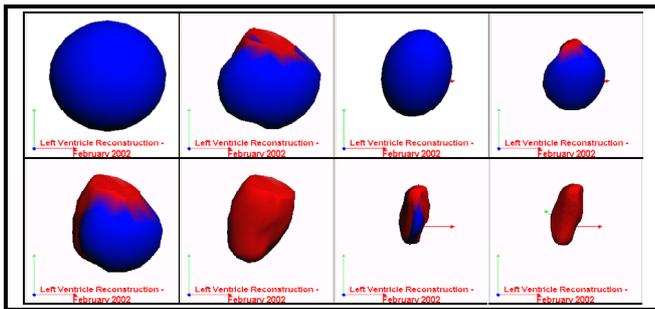Figure 8 shows the complete process for a reconstruction:

Figure 8: External (left) and internal meshes (right).

The sequence shows first the initial meshes in blue. The reconstruction begins and the meshes turn red as long as the particles reach the marked voxels.

7.6 Reconstructions with missing-data

When a patient has had a heart attack some of the areas of his heart become ischemic and, because of the absence of blood irrigation, the data we obtain can have some missing zones. We made some recovering test experiments with 10%, 32% and 53% percentages of missing volume data, always referred to the 100% of the total *PHANTOM* volume.

In these tests, a different *PHANTOM* model (more geometric heart-like) was used. Its volume was 265501 mm³. Table 4 shows the experiment.

Here the first column shows the initial data to be recovered, the second column depicts the final meshes and the third column points out the recovered final volumes (absolute values and percentage of total).

As we can see, the best recovering is the third one because it gives a percentage of missing volume of 29.1% against the 32% of the real data emptied. This represents a relative percentage error of 0.09. For the

other test examples we obtain relative errors of 0.45 and 0.24 respectively.

		Volume=265501 mm³ % of total=100%
		Volume=250944 mm³ % of total=94.5%
		Volume=188360 mm³ % of total=70.9%
		Volume=159970 mm³ % of total=60.2%

Table 4: Recovered surfaces from partial data.

8. CONCLUSIONS

We have presented the results obtained so far with *SPECT* data. In terms of precision, computing time and model accuracy, different strategies have been tested.

The final result is accurate enough for the usual medical practice. A compromise between speed and precision has to be assumed. In our present situation, we have decided to use the fastest method after testing the other approaches and checking that acceptable precision is achieved. As a function of the final application other strategies can be chosen.

9. REFERENCES

[Amatller00] J. Amatller, O. García, A. Susín. "Modelo Dinámico para la segmentación automática de imágenes 3D", X Congreso Español de Informática Gráfica-CEIG'2000, pág. 355-370, Junio 2000.

[Canny86] J. Canny. "A Computational Approach to Edge Detection", IEEE Transactions on Pattern Analysis and Machine Intelligence, Vol. 8, No. 6, Nov. 1986.

[García00] O. García, A. Susín, I. Navazo. "Segmentación Automática mediante un modelo dinámico. Aplicación a la reconstrucción del ventrículo izquierdo", Jornadas de Investigación en Ingeniería Biomédica, Sitges, 2-3 Noviembre 2000.

[García02] O. García i Panyella. "Diploma d'Estudis Avançats", Escola Tècnica Superior d'Enginyeria Electrònica i Informàtica La Salle, Universitat Ramon Llull. Març 2002.

[Susin01] A. Susín, O. García. "Modelo dinámico para la reconstrucción del corazón humano", CEDYA 2001, XVII Congreso de Ecuaciones Diferenciales y Aplicaciones y VII Congreso de Matemática Aplicada, Universidad de Salamanca, 24-28 de Septiembre de 2001.

[Xu97] C. Xu and J.L. Prince, "Gradient Vector Flow: A New External Force for Snakes", IEEE Proc. CVPR, 1997.

[Xu98] C. Xu and J.L. Prince, "Snakes, Shapes, and Gradient Vector Flow", IEEE Transactions on Image Processing, pag. 359-369, 1998.